



Electron-Acoustic Waves and Parametric Instabilities in 3-Component Relativistic Quantum Plasma with a Beam of Non-relativistic Quantum Electrons

Ikramullah¹ · Rashid Ahmad¹ · Saqib Sharif¹ · Fida Younus Khattak²

Received: 18 August 2021 / Accepted: 29 August 2023 / Published online: 19 September 2023
© The Author(s), under exclusive licence to Shiraz University 2023

Abstract

Nonlinear propagation of a highly intense circularly polarized electromagnetic wave through a 3-component relativistic quantum plasma (RQP) is studied. The plasma is composed of relativistic degenerate electrons, dynamic-degenerate ions, and a beam of non-relativistic degenerate electrons. The relativistic degenerate electrons are modeled by a *Klein–Gordon* equation (KGE), whereas the degenerate ions and beam of electrons are described by *Schrödinger* equations (SEs). The dynamics of the CPEM wave through the plasma is governed by the *Maxwell* and *Poisson* equations. Four modes have been observed through the linear analysis. It has been observed that the opacity of the plasma increases with an increase in the beam electron concentration. Stimulated Raman scattering, modulational instability, and stimulated Brillouin scattering have been studied, and an optimum value of the CPEM wave intensity has been found for the growth of these scattering instabilities. The growth rates of the SRS and SBS have been found to drop with increase in the quantum parameter (associated with the density) of the plasma. It has also been observed that the scattering spectra in both the SRS and SBS get restricted to very small wave number regions. The spectrum and the growth rate of the MI also show dependence on the quantum parameter.

Keywords 3-Component relativistic quantum plasma · Electron-acoustic waves · Nonlinear interaction of electromagnetic waves

Mathematics Subject Classification 52.25.Dg · 52.27.Cm · 52.30.Ex · 52.35.-g

1 Introduction

In an extremely dense plasma, commonly referred to as the quantum plasma, where the interparticle distance reduces to a limit such that the wave functions of the constituent particles start overlapping, particles' dynamics have to be treated quantum mechanically (Shukla and Eliasson 2011; Haas 2011; Bonitz et al. 2014). Not only in the extreme astrophysical environment where the presence of ultra-strong magnetic field in excess of the critical quantum electro-dynamical (QED) limit ($B = \frac{m_e^2 c^3}{eh} \simeq 4.4 \times 10^{13}$ G) makes the electron cyclotron energy equal to the electron rest mass energy ($m_e c^2 = 0.51$ MeV), some of the constituent particles in dense plasmas produced by the interaction of ultra-intense ($\geq 10^{21}$ W/cm²) laser pulses with matter may also acquire relativistic speed (Bonitz et al. 2014; Marklund and Shukla 2006). This necessitates the

✉ Fida Younus Khattak
fida_k@hotmail.com; fida.khattak@paf-iast.edu.pk

Ikramullah
ikramullah@kust.edu.pk

Rashid Ahmad
rashidahmad@kust.edu.pk

Saqib Sharif
saqibaan@gmail.com

¹ Department of Physics, Kohat University of Science and Technology, Kohat, Khyber Pakhtunkhwa 26000, Pakistan

² Sino-Pak Centre for Artificial Intelligence, Pak-Austria Fachhochschule: Institute of Applied Sciences and Technology, Khanpur Road Mang, Haripur, Khyber Pakhtunkhwa 22621, Pakistan

inclusion of relativistic corrections in addition to the quantum mechanical treatment in modeling the plasma dynamics. The Quark–Gluon plasmas (QGP) produced during the relativistic heavy-ion collision (RHIC) experiments (Arsene et al. 2005) is yet another example of relativistic quantum plasmas. The subject of relativistic quantum plasma (RQP) has, thus, been actively pursued by the astrophysical and plasma physics community (Melrose 2008; Asenjo et al. 2011; Mendonça 2011; Eliasson and Shukla 2011; Haas et al. 2012; Behery et al. 2016; Haas 2019; Islam et al. 2017; Singh et al. 2019; Jamil et al. 2019; Goshadze et al. 2019). Melrose (2008) has presented an excellent account of the various aspects of waves in unmagnetized relativistic-quantum plasmas using full QED formalism. This work has later been extended to include the magnetized cases (Melrose and Weise 2009, 2012).

With the help of fluid formalism, employing the *Dirac* equation for the spin-half RQP, a dispersion relation for an electromagnetic wave sustained by such a system is derived in Ref. (Asenjo et al. 2011), indicating higher transparency with the inclusion of the spin. Eliasson and Shukla (2011) have investigated the laser–plasma interactions in the relativistic quantum regime by employing a *Klein–Gordon* equation for the relativistic degenerate electrons coupled with electromagnetic waves through *Maxwell* and *Poisson* equations. Recently, we have studied (Ikramullah et al. 2017) different properties of the relativistic quantum plasma, which comprises of relativistic degenerate electrons and positrons, and dynamic degenerate ions by extending the Eliasson–Shukla model (Eliasson and Shukla 2011). It was found that the presence of positrons has insignificant effect on the dispersion. However, enhancement in the plasma opacity was observed, and the growth rate of different parametric instabilities was shown to be affected by the inclusion of positrons in the system. We further extended the model by incorporating the *Thomas–Fermi* distribution of electrons in the background of relativistic quantum plasma composed of relativistic degenerate electrons and positrons and non-relativistic degenerate ions (Ikramullah et al. 2018). An electron-acoustic wave was observed in addition to the other two modes associated with positrons and ions, respectively. The spectrum and growth rates of different instabilities were also affected with the change in the quantum parameter and with the intensity of the circularly polarized electromagnetic (CPEM) wave.

In the present work, the Eliasson–Shukla model (Eliasson and Shukla 2011) is further extended to study different physical phenomena like dispersion of electrostatic waves, self-induced transparency and plasma opacity, the occurrence and growth rates of different parametric instabilities in 3-component plasma by including a beam of non-relativistic quantum electrons along with degenerate

relativistic electrons and dynamic-degenerate ions. Ions are quantum-mechanically treated in Ref. (Shukla and Stenflo 2006) through the inclusion of *Bohm* potential, but in our case, the plasma is 3-component having two types of electrons (the relativistic degenerate electrons, and the beam of non-relativistic degenerate electrons) and the dynamic degenerate ions. The spin dynamics have not been included in the present study. We feel that the work presented in this article has relevance to both space and laboratory plasmas such as the high-density plasmas that can be produced by interacting ultrashort and ultra-intense laser pulses with solids.

This paper is organized in the following manner: in Sect. 2, a mathematical model based on the *Klein–Gordon* Equation (KGE) for relativistic degenerate electrons and *Schrödinger* Equations (SEs) for the dynamical degenerate ions and beam of non-relativistic degenerate electrons has been outlined. These equations are then coupled with the *Maxwell's* equations in order to describe the nonlinear coupling between the relativistic quantum plasma and the CPEM waves. In Sect. 3, we derive the dispersion relations by using the *Fourier* analysis and have discussed the linear properties of electrostatic oscillations. The Sect. 4 deals with the phenomena of relativistic nonlinear propagation and opacity of plasma. In Sect. 5, we study the stimulated *Raman* scattering (SRS) and modulational instabilities (MI) in a relativistic 3-component quantum plasma. In Sect. 6, we have derived the dispersion relation by considering ion dynamics and numerically studied the stimulated *Brillouin* scattering (SBS) instability. We concluded our work in Sect. 7.

2 Mathematical Model

The mathematical model of the problem composed of the KGE for the degenerate relativistic electrons, SE for the degenerate ions (beam-electrons), and *Maxwell's* and *Poisson* equations for the propagation and interaction of intense CPEM wave with the relativistic quantum plasma.

We use $\mathcal{W} = i\hbar \frac{\partial}{\partial t} + e\phi$ and $\mathbf{P} = -i\hbar\nabla + e\mathbf{A}$ in order to introduce electromagnetic interaction in KGE, given by

$$\mathcal{W}^2\psi_e - c^2\mathcal{P}^2\psi_e - m_e^2c^4\psi_e = 0. \quad (1)$$

Here, ψ_e represents an ensemble of degenerate relativistic electrons, $m_e(e)$ is an electron mass (charge), and $\phi(\mathbf{A})$ is the electromagnetic scalar (vector)-potential, respectively. In this case, the charge and current densities have the following expressions, respectively:

$$\rho_e = \frac{-e}{2m_e c^2} (\psi_e^* \mathcal{W}\psi_e + \psi_e (\mathcal{W}\psi_e)^*), \quad (2)$$

and

$$\mathbf{j}_e = \frac{-e}{2m_e} (\psi_e^* \mathbf{P} \psi_e + \psi_e (\mathbf{P} \psi_e)^*). \tag{3}$$

The coupling of an electromagnetic wave with the degenerate ions (non-relativistic beam electrons) is represented by

$$\left(i\hbar \frac{\partial}{\partial t} - q\phi \right) \psi_v = \frac{(-i\hbar \nabla - q\mathbf{A})^2}{2m_v} \psi_v, \tag{4}$$

where, the wavefunction ψ_v represents an ions ensemble (non-relativistic beam electrons), q is the charge of an ion (non-relativistic electron), and m_v is an ion (electron) mass, respectively. The electric charge and current densities of ions (non-relativistic beam-electrons) then take the following forms, respectively:

$$\rho_v = q|\psi_v|^2, \tag{5}$$

and

$$\mathbf{j}_v = \frac{iq\hbar}{2m_v} (\psi_v \nabla \psi_v^* - \psi_v^* \nabla \psi_v) - \frac{q^2}{m_v} |\psi_v|^2 \mathbf{A}. \tag{6}$$

To close the model, the scalar and vector potential (ϕ , \mathbf{A}) are obtained from the electromagnetic wave equation

$$\frac{\partial^2 \mathbf{A}}{\partial t^2} + c^2 \nabla \times (\nabla \times \mathbf{A}) + \nabla \frac{\partial \phi}{\partial t} = \mu_0 c^2 \mathbf{j}_T, \tag{7}$$

and

$$\nabla^2 \phi + \nabla \cdot \frac{\partial \mathbf{A}}{\partial t} = -\frac{1}{\epsilon_0} \left(\rho_e + \sum_{v=i,eb} \rho_v \right), \tag{8}$$

where μ_0 and ϵ_0 are the permeability and permittivity of vacuum, respectively, and $\mathbf{j}_T = \mathbf{j}_e + \sum_{v=i,eb} \mathbf{j}_v$ is the total current density. The symbol *eb* represents the beam electrons.

By taking the divergence of Eq. (7) and then using $\nabla \cdot \mathbf{A} = 0$ (*Coulomb gauge*), we obtain from Eqs. (7) and (8), respectively,

$$\nabla^2 \left(\frac{\partial^2 \mathbf{A}}{\partial t^2} - c^2 \nabla^2 \mathbf{A} \right) = -c^2 \mu_0 \nabla \times (\nabla \times \mathbf{j}_T), \tag{9}$$

and

$$\nabla^2 \phi = -\frac{1}{\epsilon_0} \left(\rho_e + \sum_{v=i,eb} \rho_v \right). \tag{10}$$

Equations (1), (9), and (10) constitute the complete model that describes the nonlinear coupling between the intense CPEM wave and the non-magnetized relativistic degenerate plasma.

3 Electrostatic Oscillations

For electrostatic waves, the electromagnetic vector potential (\mathbf{A}) is assumed to be zero. The electrostatic oscillations arise due to the charge density fluctuations in the plasma. At wavelengths comparable to the interparticle distances, the quantum effects can cause dispersion of electrostatic waves. When the wavelength associated with an electron is of the order of the *Compton* length, the electron speed becomes relativistic that can change the dispersion relation for the electrostatic waves.

To derive a dispersion relation for the electrostatic waves, we transform the wavefunction ψ_e by using the following transformation:

$$\psi_e = \tilde{\psi}_e \exp(-ic^2 m_e t / \hbar). \tag{11}$$

The modified wavefunction $\tilde{\psi}_e$ then obeys the following KGE:

$$\left(i\hbar \frac{\partial}{\partial t} + m_e c^2 + e\phi \right)^2 \tilde{\psi}_e + \hbar^2 c^2 \nabla^2 \tilde{\psi}_e - m_e^2 c^4 \tilde{\psi}_e = 0, \tag{12}$$

and the charge density of electron becomes

$$\rho_e = \frac{-ie\hbar}{2m_e c^2} \left(\tilde{\psi}_e^* \frac{\partial \tilde{\psi}_e}{\partial t} - \tilde{\psi}_e \frac{\partial \tilde{\psi}_e^*}{\partial t} \right) - \left(1 + \frac{e\phi}{m_e c^2} \right) e |\tilde{\psi}_e|^2. \tag{13}$$

The dynamics of ions (non-relativistic beam electrons) in the electrostatic case is governed by the SE:

$$i\hbar \frac{\partial \psi_v}{\partial t} - q\phi \psi_v = -\frac{\hbar^2 \nabla^2}{2m_v} \psi_v. \tag{14}$$

The ion (beam electrons) charge density is given by Eq. (5):

We linearize the system of Eqs. (10), (12), and (14) by using $\phi = \phi_1$, $\tilde{\psi}_e = \tilde{\psi}_{0e} + \tilde{\psi}_{1e}$, and $\psi_v = \psi_{0v} + \psi_{1v}$. Here, $|\tilde{\psi}_{0e}|^2 = n_{0e}$, and $|\psi_{0v}|^2 = n_{0v}$ are the unperturbed number densities of the relativistic-degenerate electrons and the degenerate ions (non-relativistic beam electrons), respectively. We *Fourier* decompose this by using $\phi_1 = \hat{\phi} \exp(i\mathbf{K} \cdot \mathbf{r} - i\Omega t) + c.c.$, $\tilde{\psi}_{1e} = \hat{\psi}_{+e} \exp(i\mathbf{K} \cdot \mathbf{r} - i\Omega t) + \hat{\psi}_{-e} \exp(-i\mathbf{K} \cdot \mathbf{r} + i\Omega t)$, and $\psi_{1v} = \psi_{+v} \exp(i\mathbf{K} \cdot \mathbf{r} - i\Omega t) + \psi_{-v} \exp(-i\mathbf{K} \cdot \mathbf{r} + i\Omega t)$.

Separating *Fourier* modes, and then eliminating the different *Fourier* coefficients, we get a dispersion relation for the electrostatic waves as follow:

$$\varepsilon = 1 + \chi_e + \sum_{v=i,eb} \chi_v = 0. \tag{15}$$

Here,

$$\chi_e = \frac{\omega_{pe}^2 (4m_e^2 c^4 - \hbar^2 (\Omega^2 - c^2 K^2))}{\hbar^2 (\Omega^2 - c^2 K^2)^2 - 4m_e^2 c^4 \Omega^2}, \tag{16}$$

and

$$\chi_v = -\frac{4\omega_{pv}^2 m_v^2}{4m_v^2 \Omega^2 - \hbar^2 K^4}, \tag{17}$$

are the electric susceptibilities of the relativistic degenerate electrons and ions (beam electrons), respectively. Here, $\omega_{pe} = (n_{0e} e^2 / \epsilon_0 m_e)^{1/2}$ and $\omega_{pv} = (n_{0v} e^2 / \epsilon_0 m_v)^{1/2}$ are, respectively, the plasma oscillation frequencies of relativistic electrons and ions (beam electrons).

To study the electron-acoustic and ion-acoustic waves associated with the low-frequency fluctuations, we apply the low-frequency limits on the Eq. (15). Assuming $\Omega < cK$, and ignoring the high powers of Ω , we obtain the following dispersion relation:

$$1 + \chi_e + \sum_{v=i,eb} \chi_v = 0. \tag{18}$$

Here,

$$\chi_e = \frac{\omega_{pe}^2 (4m_e^2 c^2 + \hbar^2 k^2)}{\hbar^2 c^2 k^4 - 4m_e^2 c^2 \Omega^2}, \tag{19}$$

is the electric susceptibility of the low-frequency electrons.

The ratio of the densities of the non-relativistic degenerate beam electrons and the relativistic degenerate electrons is denoted by β .

In Fig. 1, the solution of Eq. (15) is plotted where four different frequency branches are observed. The dashed curve is associated to the relativistic electrons having initial oscillation at the electrons plasma frequency. The dashed-dotted curve is ascribed to the ion waves, and the dotted curve represents the acoustic waves associated with the non-relativistic beam of electrons. The solid curve with the largest frequency may be attributed to the so-called ‘‘pair branch’’ or ‘‘positronic’’ states. The value of the plasma

density (hence the quantum parameter H) is chosen 10^{34} m^{-3} ($H = 0.007$) and $\beta = 10^{-5}$. We see that the phase velocity of the acoustic waves associated with the non-relativistic degenerate beam electrons is initially higher than the ion-acoustic waves and increases with a uniform rate to a certain K values beyond which it starts to decrease with a uniform rate.

In Fig. 2, Eq. (18) is plotted showing the low-frequency limit ($\Omega < cK$) for a 3-component plasma composed of the relativistic degenerate electrons, dynamic degenerate ions, and non-relativistic beam electrons by using $H = 0.007$ and $\beta = 10^{-5}$. The phase velocity of the electron-acoustic waves changes linearly in this low-frequency limit case.

We observe a behavior almost similar to what we saw in our previous studies (Ikramullah et al. 2017, 2018). The corresponding ion and the non-relativistic beam electrons wave frequencies increase as $K \rightarrow 0$ by increasing the value of the quantum parameter. The beam and ion modes, both, behave in the same way. However, in this case, the low-frequency waves resulted from the beam of electrons are lower in frequency as compared to the low-frequency waves in the *Thomas–Fermi* distributed electrons (Ikramullah et al. 2018). Similarly, the frequency of ion-acoustic waves is also lower in the beam case than the *Thomas–Fermi* case.

4 Nonlinear Propagation of Intense Electromagnetic Waves Through Degenerate Plasma

We use the *Klein–Gordon–Schrödinger–Maxwell* model to study the propagation of intense CPEM wave through the 3-component plasma. We consider nonlinear effects produced from the coupling of a CPEM wave $\mathbf{A} = A_0 [\hat{x} \cos(kz - \omega t) - \hat{y} \sin(kz - \omega t)]$ with the 3-component relativistic degenerate plasma. Here, ω and k are the

Fig. 1 Dispersion curves, obtained by plotting the solution of Eq. (15), for a plasma consisting of relativistic degenerate electrons, dynamic degenerate ions, and non-relativistic electrons beam for $H = 0.007$ and $\beta = 10^{-5}$

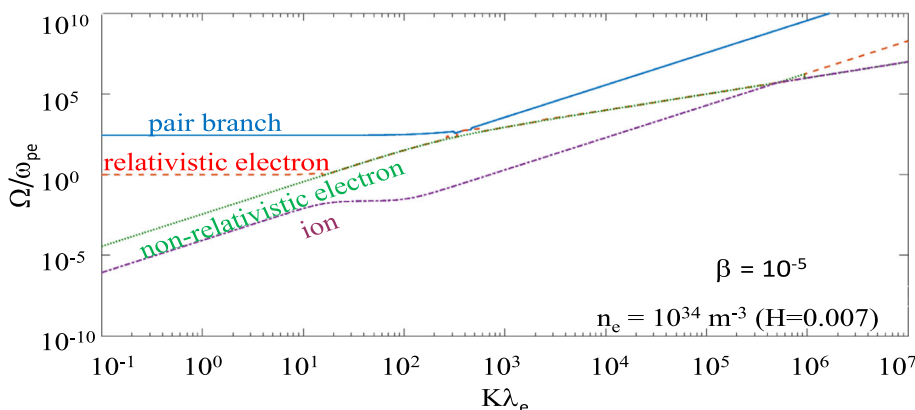
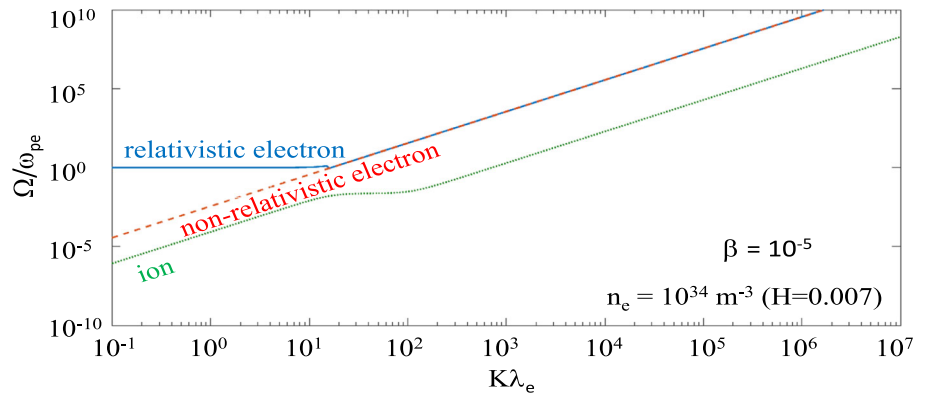


Fig. 2 Figure showing the dispersion in the low-frequency limit, obtained by plotting the solution of Eq. (18), using $H = 0.007$ and $\beta = 10^{-5}$



angular frequency and wave number of the incident electromagnetic wave. We choose CPWM wave in a manner that the nonlinear term, which is proportional to A^2 in the KGE and SEs, vanish. It is further assumed that the plasmas oscillate transversely to the propagation direction of electromagnetic wave and, therefore, we put $\phi = 0$. Further, assuming that ψ_e and ψ_v are time dependent only, we get the following equations from the KGE. (1) and SE (4), respectively:

$$\hbar^2 \frac{\partial^2 \psi_e}{\partial t^2} + c^2 (-i\hbar \nabla + e\mathbf{A})^2 \psi_e + m_e^2 c^4 \psi_e = 0, \quad (20)$$

and

$$i\hbar \frac{\partial \psi_v}{\partial t} = \frac{q^2 A^2}{2m_v} \psi_v. \quad (21)$$

By putting the value of \mathbf{A} , and further simplifying the above equations Eqs. (20) and (23), we get

$$\hbar^2 \frac{\partial^2 \psi_e}{\partial t^2} + m_e^2 c^4 \gamma_A \psi_e = 0, \quad (22)$$

and

$$i\hbar \frac{\partial \psi_v}{\partial t} = \frac{q^2 A_0^2}{2m_v} \psi_v. \quad (23)$$

Here, $\gamma_A = \left(1 + e^2 A_0^2 / m_e^2 c^2\right)^{1/2}$ is the relativistic gamma factor signifying an increase in the mass of electron due to interaction with the intense CPWM waves. The solution of Eqs. (22) and (23) are:

$$\psi_e = \psi_{0e} \exp(-im_e c^2 \gamma_A t / \hbar), \quad (24)$$

$$\psi_v = \psi_{0v} \exp(-ie^2 A_0^2 t / 2m_v \hbar). \quad (25)$$

The electron number density in equilibrium can be determined by putting Eq. (24) in Eq. (2), and using $\rho_e = -en_{0e}$ as,

$$|\psi_{0e}|^2 = n_{0e} / \gamma_A. \quad (26)$$

Similarly, the unperturbed ion (non-relativistic beam

electrons) number density is calculated by putting $\rho_v = qn_{0v}$ and Eq. (25) in Eq. (5),

$$|\psi_{0v}|^2 = n_{0v}. \quad (27)$$

The current densities are calculated by using Eq. (24) in Eq. (3) and Eq. (25) in Eq. (6) as

$$\mathbf{J}_e = -\frac{e^2 |\psi_{0e}|^2}{m_e} \mathbf{A} = -\frac{e^2 n_{0e}}{\gamma_A m_e} \mathbf{A}, \quad (28)$$

and

$$\mathbf{J}_v = -\frac{q^2 |\psi_{0v}|^2}{m_v} \mathbf{A} = -\frac{q^2 n_{0v}}{m_v} \mathbf{A}. \quad (29)$$

Using Eqs. (28) and (29), and the expression of total current density \mathbf{J}_T in Eq. (9), we get the following relation:

$$\frac{1\partial^2 \mathbf{A}}{c^2 \partial t^2} - \nabla^2 \mathbf{A} = -\frac{\mu_0 e^2 n_{0e}}{\gamma_A m_e} \mathbf{A} - \frac{\mu_0 q^2 n_{0v}}{m_v} \mathbf{A}. \quad (30)$$

By putting the value of \mathbf{A} in Eq. (30), we get the nonlinear dispersion relation as in follow:

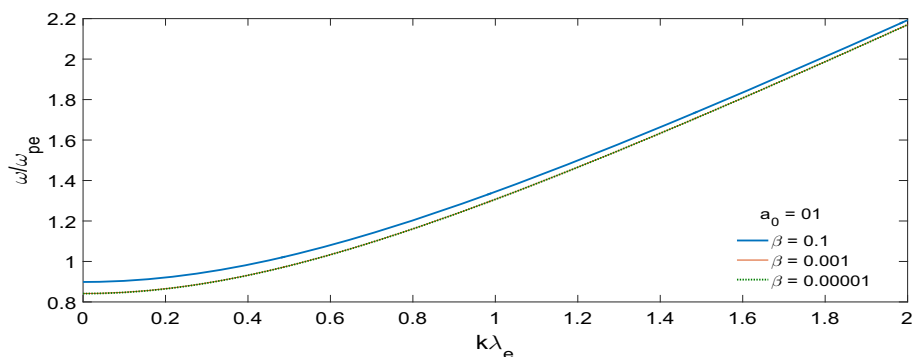
$$\omega^2 = k^2 c^2 + \frac{\omega_{pe}^2}{\gamma_A} + \sum_{v=i,eb} \omega_{pv}^2. \quad (31)$$

If ions are considered to be static, the nonlinear dispersion relation changes to the following relation:

$$\omega^2 = k^2 c^2 + \frac{\omega_{pe}^2}{\gamma_A} + \omega_{peb}^2. \quad (32)$$

Figure 3 shows the dispersion of carrier waves for different β (non-relativistic quantum beam electrons concentration) at fixed wave amplitude. It is observed that the opacity of the plasma increases with the increase in β .

Fig. 3 Plots showing dispersion of incident waves for $(\beta = 0.00001, 0.001, 0.1)$ and $a_0 = 01$



5 Stimulated Raman Scattering and Modulational Instabilities

In the simulated Raman scattering (SRS), the decay of CPEM wave results in a scattered electromagnetic wave and an electron plasma wave. We assume the ions to be static, serving as a uniform neutralizing background. For simplicity, we introduce the transformation $\psi_e = \tilde{\psi}_e \exp(-im_e \gamma_A c^2 t / \hbar)$, where $\gamma_A = \sqrt{1 + e^2 A_0^2 / m_e^2 c^2}$ is the gamma factor and A_0 is the amplitude of the incident CPEM wave. The modified wave function $\tilde{\psi}_e$ then obeys the KGE in the following form:

$$\left(i\hbar \frac{\partial}{\partial t} + \gamma_A m_e c^2 + e\phi \right)^2 \tilde{\psi}_e - c^2 (-i\hbar \nabla + e\mathbf{A})^2 \tilde{\psi}_e - m_e^2 c^4 \tilde{\psi}_e = 0, \tag{33}$$

The charge density then takes the following form:

$$\rho_e = \frac{-ie\hbar}{2m_e c^2} \left(\tilde{\psi}_e^* \frac{\partial \tilde{\psi}_e}{\partial t} - \tilde{\psi}_e \frac{\partial \tilde{\psi}_e^*}{\partial t} \right) - \left(\gamma_A + \frac{e\phi}{m_e c^2} \right) e |\tilde{\psi}_e|^2. \tag{34}$$

The system of Eqs. (4), (9), (10), (33), and (34) in the SRS case are linearized by using $\tilde{\psi}_e(\mathbf{r}, t) = \tilde{\psi}_{0e} + \tilde{\psi}_{1e}(\mathbf{r}, t)$, $\psi_{eb}(\mathbf{r}, t) = \psi_{0eb} + \psi_{1eb}(\mathbf{r}, t)$, $\mathbf{A}(\mathbf{r}, t) = \mathbf{A}_0(\mathbf{r}, t) + \mathbf{A}_1(\mathbf{r}, t)$ and $\phi(\mathbf{r}, t) = \phi_1(\mathbf{r}, t)$ to obtain the following linearized equations:

$$\begin{aligned} & \hbar^2 \left(-\frac{\partial^2 \tilde{\psi}_{1e}}{\partial t^2} + c^2 \nabla^2 \tilde{\psi}_{1e} \right) + 2i\hbar \gamma_A m_e c^2 \frac{\partial \tilde{\psi}_{1e}}{\partial t} \\ & + 2i\hbar c^2 e \mathbf{A}_0 \cdot \nabla \tilde{\psi}_{1e} + e \left(2\gamma_A m_e c^2 \phi_1 + i\hbar \frac{\partial \phi_1}{\partial t} \right) \tilde{\psi}_{0e} \\ & - 2c^2 e^2 \mathbf{A}_0 \cdot \mathbf{A}_1 \tilde{\psi}_{0e} = 0, \end{aligned} \tag{35}$$

$$\begin{aligned} \nabla^2 \phi_1 &= \frac{ie\hbar}{2\epsilon_0 m_e c^2} \left(\tilde{\psi}_{0e}^* \frac{\partial \tilde{\psi}_{1e}}{\partial t} - \tilde{\psi}_{0e} \frac{\partial \tilde{\psi}_{1e}^*}{\partial t} \right) \\ & + \frac{e\gamma_A}{\epsilon_0} \left(\tilde{\psi}_{0e}^* \tilde{\psi}_{1e} + \tilde{\psi}_{1e}^* \tilde{\psi}_{0e} \right) + \frac{\omega_{pe}^2}{\gamma_A c^2} \phi_1 \\ & + \frac{e}{\epsilon_0} \left(\psi_{0eb}^* \psi_{1eb} + \psi_{1eb}^* \psi_{0eb} \right), \end{aligned} \tag{36}$$

$$i\hbar \frac{\partial \psi_{eb}}{\partial t} + e\psi_{0eb} \phi_1 = \frac{1}{2m_e} \left(-\hbar^2 \nabla^2 + 2e^2 \psi_{0eb} \mathbf{A}_0 \cdot \mathbf{A}_1 \right) \psi_{eb} \tag{37}$$

$$\begin{aligned} \nabla^2 \left(\frac{\partial^2 \mathbf{A}_1}{\partial t^2} - c^2 \nabla^2 \mathbf{A}_1 + \frac{\omega_{pe}^2}{\gamma_A} \mathbf{A}_1 + \omega_{peb}^2 \mathbf{A}_1 \right) \\ = \frac{\omega_{pe}^2}{n_{0e}} \nabla \times \left(\nabla \times \left(\mathbf{A}_0 \left(\tilde{\psi}_{0e}^* \tilde{\psi}_{1e} + \tilde{\psi}_{1e}^* \tilde{\psi}_{0e} \right) \right) \right) \\ + \frac{\omega_{peb}^2}{n_{0eb}} \nabla \times \left(\nabla \times \left(\mathbf{A}_0 \left(\psi_{0eb}^* \psi_{1eb} + \psi_{1eb}^* \psi_{0eb} \right) \right) \right) \end{aligned} \tag{38}$$

The term $\mathbf{A}_0 \cdot \nabla \tilde{\psi}_{1e}$ in the Eq. (35) is associated with the two-plasmon decay, which will not be considered in this study. In what follows, we use the following Fourier representations: $\tilde{\psi}_{1e} = \hat{\psi}_{+e} \exp[i(\mathbf{K} \cdot \mathbf{r} - \Omega t)] + \hat{\psi}_{-e} \exp[-i(\mathbf{K} \cdot \mathbf{r} - \Omega t)]$, $\psi_{1eb} = \hat{\psi}_{+eb} \exp[i(\mathbf{K} \cdot \mathbf{r} - \Omega t)] + \hat{\psi}_{-eb} \exp[-i(\mathbf{K} \cdot \mathbf{r} - \Omega t)]$, $\phi_1 = \hat{\phi} \exp[i(\mathbf{K} \cdot \mathbf{r} - \Omega t)] + c.c.$, $\mathbf{A}_0 = (1/2) \hat{\mathbf{A}}_0 \exp[i(\mathbf{k}_0 \cdot \mathbf{r} - \omega_0 t)] + c.c.$ and $\mathbf{A}_1 = \hat{\mathbf{A}}_+ \exp[i(\mathbf{k}_+ \cdot \mathbf{r} - \omega_+ t)] + \hat{\mathbf{A}}_- \exp[-i(\mathbf{k}_- \cdot \mathbf{r} - \omega_- t)] + c.c.$ where $\omega_{\pm} = \omega_0 \pm \Omega$ and $\mathbf{k}_{\pm} = \mathbf{k}_0 \pm \mathbf{K}$.

Now Fourier decomposing Eqs. (35), (36), (37), and (38), and eliminating different Fourier coefficients, we get the dispersion relation as follows:

$$\begin{aligned}
 1 + \frac{\gamma_A B}{\omega_{pe}^2} - \frac{4\gamma_A \omega_{peb}^2 m_e^2 B}{\omega_{pe}^2 AC} &= \left[\frac{(-\Omega^2 + \omega_{pe}^2/\gamma_A)}{A} + \right. \\
 &\frac{4\omega_{peb}^2 m_e^2 \Omega^2}{AC} + \frac{\omega_{peb}^2 K^2 \hbar^2 \Omega'^2}{c^2 AC} - \frac{4\gamma_A^2 m_e^2 c^2 K^2 \omega_{peb}^2}{AC} + \\
 &\left. \frac{8\gamma_A \omega_{peb}^2 c^2 K^2 m_e^2}{AC} - \frac{\gamma_A \omega_{peb}^2 K^2 (\hbar^2 \Omega'^4 - 4\gamma_A^2 m_e^2 c^4 \Omega^2)}{c^2 \omega_{pe}^2 AC} \right] \\
 &\times c^2 e^2 M', \tag{39}
 \end{aligned}$$

where

$$\begin{aligned}
 M' &= \frac{|\mathbf{k}_+ \times \hat{\mathbf{A}}_0|^2}{\mathbf{k}_+^2 D_A(\omega_+, \mathbf{k}_+)} + \frac{|\mathbf{k}_- \times \hat{\mathbf{A}}_0|^2}{\mathbf{k}_-^2 D_A(\omega_-, \mathbf{k}_-)}, \\
 A &= (4\gamma_A^2 m_e^2 c^4 - \hbar^2 \Omega'^2), \\
 B &= (\hbar^2 \Omega'^4 - 4\gamma_A^2 m_e^2 c^4 \Omega^2), \\
 C &= (4m_e^2 \Omega^2 - \hbar^2 K^4), \\
 \Omega'^2 &= (\Omega^2 - c^2 K^2).
 \end{aligned}$$

Here, relation $D_A(\omega_{\pm}, k_{\pm}) = c^2 k_{\pm}^2 - \omega_{\pm}^2 + \omega_{pe}^2/\gamma_A + \omega_{peb}^2$ governs the electromagnetic side-bands.

To evaluate the nonlinear dispersion relation Eq. (39) numerically, we use a coordinate system such that $\mathbf{k}_0 = k_0 \hat{\mathbf{z}}$ and $\hat{\mathbf{A}}_0 = A_0(\hat{\mathbf{x}} + i\hat{\mathbf{y}})$. We take $\mathbf{K} = K_{\parallel} \hat{\mathbf{z}} + K_{\perp} \hat{\mathbf{y}}$. Therefore, we have $K^2 = K_{\perp}^2 + K_{\parallel}^2$, $\gamma_A = \sqrt{(1 + e^2 |\hat{\mathbf{A}}_0|^2/m_e^2 c^2)}$, $|\mathbf{k}_{\pm} \times \hat{\mathbf{A}}_0|^2 = |\hat{\mathbf{A}}_0|^2 [2(k_0 \pm K_{\parallel})^2 + K_{\perp}^2]$ and $k_{\pm}^2 = K_{\perp}^2 + (k_0 \pm K_{\parallel})^2$. The incident wave \mathbf{A}_0 obeys the nonlinear dispersion relation given by: $\omega_0 = \sqrt{c^2 k_0^2 + \omega_{peb}^2 + \omega_{pe}^2/\gamma_A}$.

Now, we assume that $\Omega = \Omega_R + i\Omega_I$, where Ω_R and Ω_I are the real part of the frequency and the growth rate, respectively, and we solve the Eq. (39) numerically.

In Fig. 4, we have shown the growth rate of the SRS instability in the 3-component relativistic quantum plasma with quantum parameter $H = 0.007$ for different CPEM wave amplitudes. As was observed in Refs. (Eliasson and Shukla 2011; Ikramullah et al. 2017) for the 2- and 3-component plasma, we observe a spread in the spectrum with the increasing amplitude of the CPEM wave. The growth rate increases with an increase in the amplitude of the CPEM wave and has an optimum value at $a_0 = 05$.

Figure 5 shows the growth rate of the MI at various wave amplitudes, and at quantum parameter $H = 0.007$. As was noticed in the case of the Raman scattering, one can see that both the spectrum and the growth rate reaches to an optimum value at $a_0 = 5.0$ and then drops as one moves to the higher CPEM wave amplitudes.

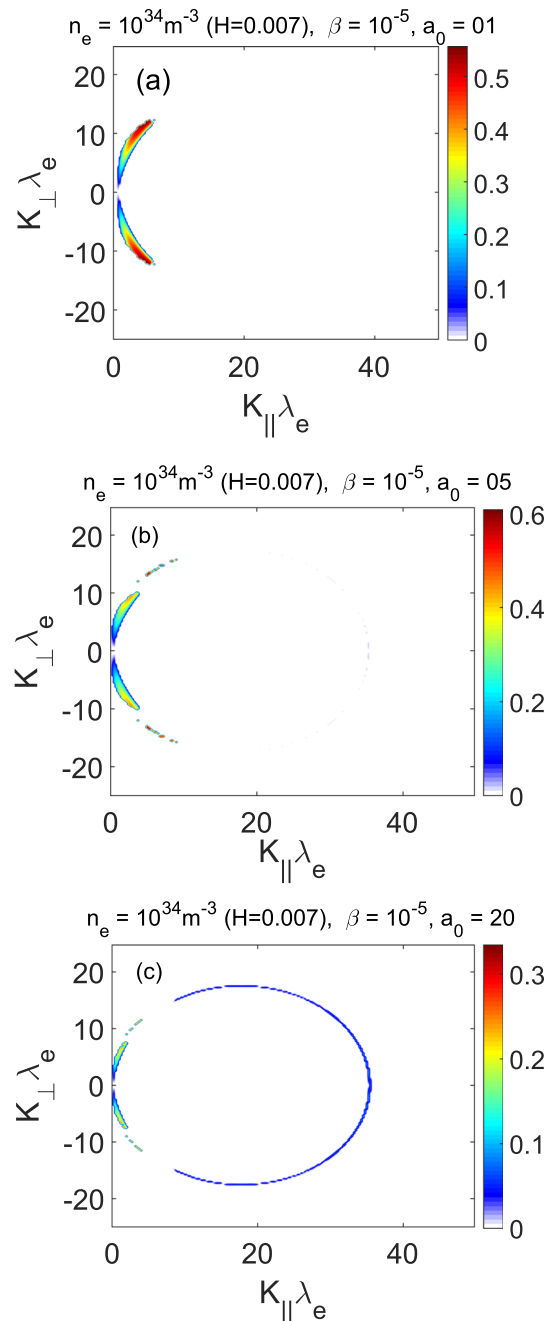


Fig. 4 Plots displaying the SRS growth rate as function of the wavenumbers K_{\parallel} and K_{\perp} for $H = 0.007$, for CPEM amplitudes $a_0 = 1.0, 5.0, 20.0$, and for the beam electrons concentration, $\beta = 10^{-5}$

6 Stimulated Brillouin (SBS) Scattering

In the SBS instability, an incident electromagnetic wave changes to a low-frequency ion-acoustic wave associated with the ions density fluctuations and a high-frequency scattered electromagnetic wave. In the 3-component plasma undertaken here, the KGE describes the collective

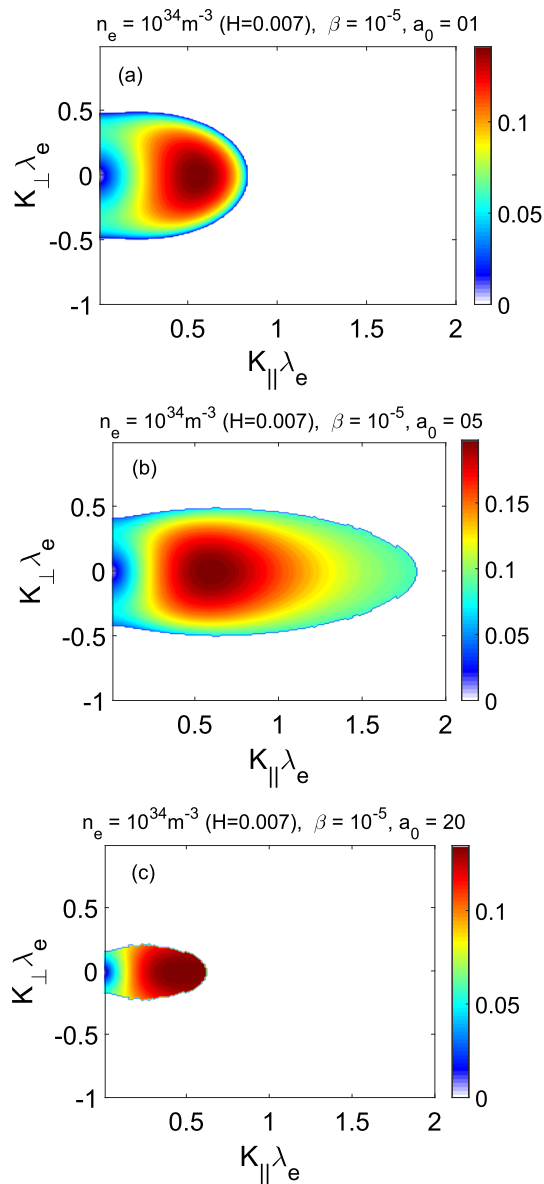


Fig. 5 Plots depicting the growth rate of the MI as a function of the wave numbers K_{\parallel} and K_{\perp} for CPEM amplitude of $a_0 = 1.0, 5.0, 20$, quantum parameter $H = 0.007$, and beam electrons concentration, $\beta = 10^{-5}$

oscillatory motion of electrons in the plasma. The linearized KGE for electrons coupled with the CPEM waves is given by Eq. (35). The ions (non-relativistic beam electrons) dynamics is modeled by the *Schrödinger* equation coupled to the CPEM wave through *Poisson* and *Maxwell* equations. By using $\tilde{\psi}_v(\mathbf{r}, t) = \tilde{\psi}_{0v} + \tilde{\psi}_{1v}(\mathbf{r}, t)$, $\phi(\mathbf{r}, t) = \phi_1(\mathbf{r}, t)$ and $\mathbf{A}(\mathbf{r}, t) = \mathbf{A}_0(\mathbf{r}, t) + \mathbf{A}_1(\mathbf{r}, t)$, the linearized *Schrödinger* equation is rewritten here while neglecting the term proportional to the Two-Plasmon Decay.

$$i\hbar \frac{\partial}{\partial t} \psi_{1v} - q\psi_{0v}\phi_1 = \frac{1}{2m_v} (-\hbar^2 \nabla^2 \psi_{1v} + 2c^2 \psi_{0v} \mathbf{A}_0 \cdot \mathbf{A}_1) \quad (40)$$

The linearized wave and *Poisson* equations given by Eqs. (9) and (10) in case of dynamical ions then take the following form:

$$\begin{aligned} \nabla^2 \phi_1 = & \frac{ie\hbar}{2\epsilon_0 m_e c^2} \left(\tilde{\psi}_{0e}^* \frac{\partial \tilde{\psi}_{1e}}{\partial t} - \tilde{\psi}_{0e} \frac{\partial \tilde{\psi}_{1e}^*}{\partial t} \right) \\ & + \frac{e\gamma_A}{\epsilon_0} (\tilde{\psi}_{0e}^* \tilde{\psi}_{1e} + \tilde{\psi}_{1e}^* \tilde{\psi}_{0e}) + \frac{\omega_{pe}^2}{\gamma_A c^2} \phi_1 \\ & - \sum_{v=i,eb} \frac{q}{\epsilon_0} (\psi_{0v} \psi_{1v}^* + \psi_{0v}^* \psi_{1v}), \end{aligned} \quad (41)$$

and

$$\begin{aligned} \nabla^2 \left(\frac{\partial^2 A_1}{\partial t^2} - c^2 \nabla^2 A_1 + \frac{\omega_{pe}^2}{\gamma_A} A_1 + \sum_{v=i,eb} \omega_{pv}^2 A_1 \right) \\ = \frac{\omega_{pe}^2}{n_{0e}} \nabla \times (\nabla \times (A_0 (\tilde{\psi}_{0e}^* \tilde{\psi}_{1e} + \tilde{\psi}_{1e}^* \tilde{\psi}_{0e}))) \\ + \sum_{v=i,eb} \frac{\omega_{pv}^2}{n_{0v}} \nabla \times (\nabla \times (A_0 (\psi_{0v} \psi_{1v} + \psi_{1v}^* \psi_{0v}))). \end{aligned} \quad (42)$$

Now *Fourier* decomposing the above equations by using $\psi_{1v} = \hat{\psi}_{+v} \exp[i(\mathbf{K} \cdot \mathbf{r} - \Omega t)] + \hat{\psi}_{-v} \exp[-i(\mathbf{K} \cdot \mathbf{r} - \Omega t)]$, $\phi_1 = \hat{\phi} \exp[i(\mathbf{K} \cdot \mathbf{r} - \Omega t)] + c.c.$, $\tilde{\psi}_e = \hat{\psi}_{+e} \exp[i(i\mathbf{K} \cdot \mathbf{r} - i\Omega t)] + \hat{\psi}_{-e} \exp[-i(\mathbf{K} \cdot \mathbf{r} - i\Omega t)]$, $\mathbf{A}_0 = \frac{1}{2} \hat{\mathbf{A}}_0 \exp[i(\mathbf{k}_0 \cdot \mathbf{r} - \omega_0 t)] + c.c.$, $\mathbf{A}_1 = \hat{\mathbf{A}}_+ \exp[i(\mathbf{k}_+ \cdot \mathbf{r} - \omega_+ t)] + \hat{\mathbf{A}}_- \exp[i(\mathbf{k}_- \cdot \mathbf{r} - \omega_- t)] + c.c.$, where $\omega_{\pm} = \omega_0 \pm \Omega$ and $\mathbf{k}_{\pm} = \mathbf{k}_0 \pm \mathbf{K}$ and *c.c.* denotes the complex conjugate.

We now separate the *Fourier* modes by using the *Fourier* decomposition in Eqs. (35), (40), (41), and (42), and eliminating different *Fourier* coefficients, we get the nonlinear dispersion relation in the following form:

$$\begin{aligned} 1 + \frac{\gamma_A B}{\omega_{pe}^2 A} - \frac{4\gamma_A \omega_{pi}^2 m_i^2 B}{\omega_{pe}^2 A D} - \frac{4\gamma_A \omega_{peb}^2 m_e^2 B}{\omega_{pe}^2 A C} = \\ \left[\frac{(-\Omega^2 + \omega_{pe}^2/\gamma_A)}{A} + \frac{4\omega_{pi}^2 m_i^2 \Omega^2}{A D} + \frac{\omega_{pi}^2 K^2 \hbar^2 \Omega^2}{c^2 A D} - \frac{4\gamma_A^2 m_e^2 c^2 K^2 \omega_{pi}^2}{A D} - \frac{8\gamma_A \omega_{pi}^2 c^2 K^2 m_e m_i}{A D} - \frac{\gamma_A \omega_{pi}^2 K^2 B}{c^2 \omega_{pe}^2 A D} + \frac{4\omega_{peb}^2 m_e^2 \Omega^2}{A C} + \frac{\omega_{peb}^2 K^2 \hbar^2 \Omega^2}{c^2 A C} - \frac{4\gamma_A^2 m_e^2 c^2 K^2 \omega_{peb}^2}{A C} + \frac{8\gamma_A \omega_{peb}^2 c^2 K^2 m_e^2}{A C} - \frac{\gamma_A \omega_{peb}^2 K^2 B}{c^2 \omega_{pe}^2 A C} + \frac{4\gamma_A \omega_{pi}^2 \omega_{peb}^2 K^2 (m_e + m_i)^2 B}{c^2 \omega_{pe}^2 A C D} \right] \times c^2 e^2 M', \end{aligned} \quad (43)$$

where

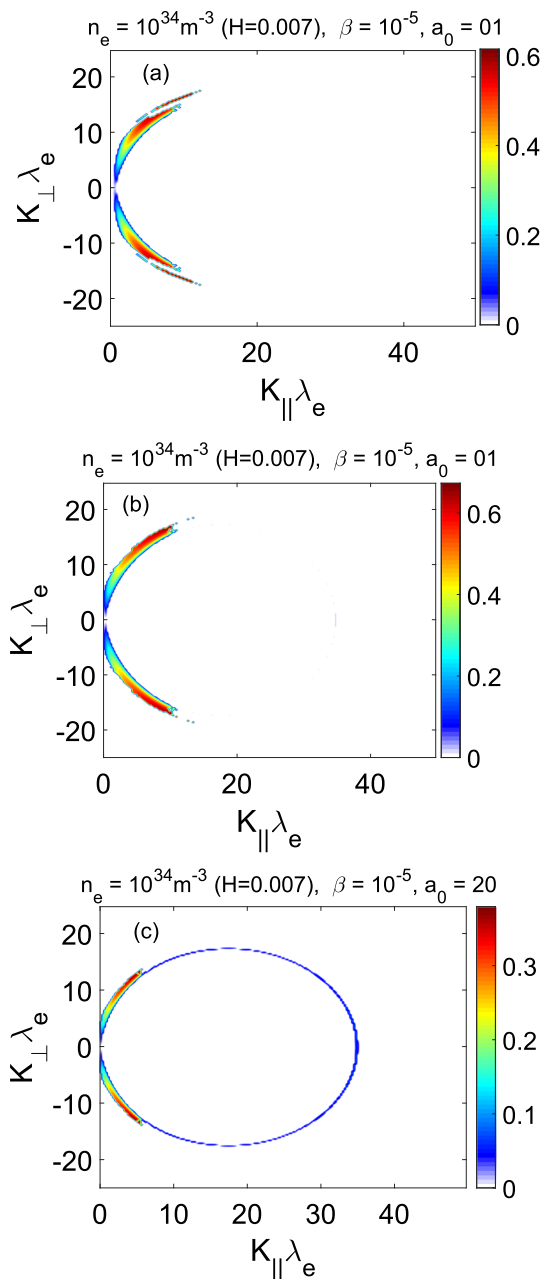


Fig. 6 Figure depicting the growth rate of the SBS as a function of the wavenumbers K_{\parallel} and K_{\perp} for the quantum parameter $H = 0.007$, CPEM amplitude $a_0 = 1.0, 5.0, 20.0$ and beam concentration, $\beta = 10^{-5}$

$$M' = \frac{|\mathbf{k}_+ \times \hat{\mathbf{A}}_0|^2}{k_+^2 D_A(\omega_+, \mathbf{k}_+)} + \frac{|\mathbf{k}_- \times \hat{\mathbf{A}}_0|^2}{k_-^2 D_A(\omega_-, \mathbf{k}_-)},$$

$$D = (4m_i^2 \Omega^2 - \hbar^2 K^4).$$

Here, $D_A(\omega_{\pm}, \mathbf{k}_{\pm}) = c^2 k_{\pm}^2 - \omega_{\pm}^2 + \sum_{v=i,eb} \omega_{pv}^2 + \omega_{pe}^2 / \gamma_A$ governs the electromagnetic sidebands.

In case of SBS, $\Omega \ll cK$, therefore, we neglect Ω^2 and its higher powers. We, therefore, get the following expression from the nonlinear dispersion relation Eq. (43):

$$1 + \frac{\gamma_A c^2 E}{\omega_{pe}^2 F} - \frac{4\gamma_A \omega_{pi}^2 m_i^2 c^2 E}{\omega_{pe}^2 ED} - \frac{4\gamma_A \omega_{peb}^2 m_e^2 c^2 E}{\omega_{pe}^2 FC}$$

$$= \left[\frac{(c^2 K^2 + \omega_{pe}^2 / \gamma_A)}{c^2 F} - \frac{4\omega_{pi}^2 m_i^2 K^2}{FD} - \frac{\omega_{pi}^2 K^4 \hbar^2}{c^2 FD} \right.$$

$$- \frac{4\gamma_A^2 m_e^2 K^2 \omega_{pi}^2}{(FD)} - \frac{8\gamma_A \omega_{pi}^2 K^2 m_e m_i}{FD} - \frac{\gamma_A \omega_{pi}^2 K^2 E}{c^2 \omega_{pe}^2 FD}$$

$$- \frac{4\omega_{peb}^2 m_e^2 K^2}{FC} - \frac{\omega_{peb}^2 K^4 \hbar^2}{c^2 FC} - \frac{4\gamma_A^2 m_e^2 K^2 \omega_{peb}^2}{FC}$$

$$+ \frac{8\gamma_A \omega_{pb}^2 K^2 m_e m_e}{(4\gamma_A^2 m_e^2 c^2 + \hbar^2 K^2)(4m_e^2 \Omega^2 - \hbar^2 K^4)} - \frac{\gamma_A \omega_{peb}^2 K^2 E}{c^2 \omega_{pe}^2 FC}$$

$$\left. + \frac{4\gamma_A \omega_p^2 \omega_{peb}^2 K^2 (m_e + m_i)^2 E}{\omega_{pe}^2 FDC} \right] \times c^2 e^2 M'',$$

where

$$M'' = \frac{|\mathbf{k}_+ \times \hat{\mathbf{A}}_0|^2}{k_+^2 (c^2 k_+^2 - (\omega_0^2 + 2\omega_0 \Omega) + \omega_{pe}^2 / \gamma_A + \sum_{v=i,eb} \omega_{pv}^2)} +$$

$$\frac{|\mathbf{k}_- \times \hat{\mathbf{A}}_0|^2}{k_-^2 (c^2 k_-^2 - (\omega_0^2 - 2\omega_0 \Omega) + \omega_{pe}^2 / \gamma_A + \sum_{v=i,eb} \omega_{pv}^2)},$$

$$E = (\hbar^2 K^4 - 4\gamma_A^2 m_e^2 \Omega^2),$$

$$F = (4\gamma_A^2 m_e^2 c^2 + \hbar^2 K^2).$$

To solve Eq. (44) numerically, we use the same coordinate system as was used in the case of SRS and we simplify various expressions in a fashion similar to what employed in the case of Eq. (39).

From Fig. 6, we observe that the spectrum spreads with the increasing values of the CPEM amplitude, and the growth rate is maximum at $a_0 = 05$. We also note that the growth rate of the instability enhances and that the spectrum spreads with an increase in the beam electrons concentration.

Our study shows a signature of strong correlation between the growth rates of these instabilities and the relativistic quantum parameter H . This suggests a strong association between the particles collective motion at the quantum scale and the dispersive properties of the plasma, thus, affecting the growth rates of the parametric instabilities as was earlier observed by Shukla and Stenflo Ref. (Shukla and Stenflo 2006).

7 Conclusion

The extension of the models developed in Refs. (Eliasson and Shukla 2011; Ikramullah et al. 2017) is carried out for the 3-component relativistic quantum plasma comprising of relativistic degenerate electrons, dynamic degenerate ions, and non-relativistic quantum beam of electrons. The KGE is used for the relativistic degenerate electrons, while the dynamical degenerate ions and the non-relativistic beam of degenerate electrons are modeled through the SEs. Four modes have been observed in the dispersion. These modes are affected by a change in the quantum parameter (the density) of the plasma. The interaction of the intense CPEM waves with the 3-component quantum plasma shows that while an increase in the CPEM amplitude leads to self-induced transparency due to the relativistic mass increase, the addition of non-relativistic degenerate electron beam increases the plasma opacity. The growth rates of both the SRS and the SBS instabilities reduce with an increase in the quantum parameter H , and the scattering spectra get restricted to small wave-number regions. Whereas the spectra of these parametric instabilities remain largely insensitive to the changes in the beam concentration for small amplitude CPEM waves, the spectra change significantly with a change in the beam concentration when CPEM waves of large amplitude interact with the 3-component plasma. Furthermore, the growth rates increase with an increase in the non-relativistic electrons beam concentration. The width of the scattering spectra increases with an increase in the amplitudes of the CPEM wave. The growth-rate first enhances and then reduces with the increasing intensity of the CPEM wave. The growth rate of the MI also shows dependence on the quantum parameter as well as on the beam concentration.

Acknowledgements The authors gratefully acknowledge the financial support of the Higher Education Commission of Pakistan through the Start-up Research Grant Program. Project No: 21-2181/SRGP/R &D//HEC/2018.

Author Contributions I did analytical modeling, data curation/analysis, simulation, and draft manuscript. RA performed conceptualization, analytical modeling, and editing. SS carried out MATLAB simulation. FYK analyzed conceptualization, modeling, analysis, writing/editing/proofreading, and submission of the manuscript for publication.

Funding The authors have not disclosed any funding.

Data Availability The data that support the plots and other findings of this study are available from the corresponding author upon reasonable request.

Declarations

Conflict of interest The authors declare that they have neither any known competing financial interests nor personal relationships that could have appeared to influence in any manner the work reported in this paper.

Consent for Publication All the authors submit their full consent to the Iranian Journal of Science for publication of the work presented in this article.

Consent to Participate No participation of human being or animal as subject for data in this study.

Ethical Approval I, Prof Fida Younus Khattak, on my own behalf and on behalf of my co-authors assure that the following is fulfilled for the manuscript “Electronacoustic waves and parametric instabilities in 3-component relativistic quantum plasma with a beam of non-relativistic quantum electrons.” The manuscript is resulted from original work/research analyzed in a truthful manner that has neither been previously published in any journal nor is currently being considered for publication elsewhere. Proper credit has been given to the co-researchers. All the coauthors have made substantial contribution and all of us take public responsibility for the contents of the article. The results are placed appropriately in the context of the relevant published research with correct citation. Through this statement, we declare that this submission is in accordance with the ethical policies of the Iranian Journal of Science. We are aware of the consequences for violation of the Ethical Statement or a part.

References

- Arsene I, Bearden IG, Beavis D, Besliu C, Budick C, Bøggild H, Chasman C, Christensen CH, Christiansen P, Cibor J, Debye R, Enger E, Gaardhøje JJ, Germinario M, Hansen O, Holm A, Holme A, Hagel K, Ito H, Jakobsen E, Jipa A, Jundt F, Jørdre J, Jørgensen CE, Karabowicz R, Kim EJ, Kozik T, Larsen TM, Lee JH, Lee YK, Lindahl S, Løvholden G, Majka Z, Makeev A, Mikelsen M, Murray M, Natowitz J, Neumann B, Nielsen BS, Ouerdane D, Planeta R, Rami F, Ristea C, Ristea O, Röhrich D, Samset BH, Sandberg D, Sanders SJ, Scheetz RA, Staszal P, Tsveter T, Videbæk F, Wada R, Yin Z, Zgura IS (2005) Quark-gluon plasma and color glass condensate at rhic? the perspective from the brahms experiment. *Nucl Phys A* 757(1):1–27. <https://doi.org/10.1016/j.nuclphysa.2005.02.130>
- Asenjo FA, Muñoz V, Valdivia JA, Mahajan SM (2011) A hydrodynamical model for relativistic spin quantum plasmas. *Phys Plasmas* 18(1):012107. <https://doi.org/10.1063/1.3533448>
- Behery EE, Haas F, Kourakis I (2016) Weakly nonlinear ion-acoustic excitations in a relativistic model for dense quantum plasma. *Phys Rev E* 93:023206. <https://doi.org/10.1103/PhysRevE.93.023206>
- Bonitz M, Lopez J, Becker K, Thomsen H (2014) Complex plasmas: scientific challenges and technological opportunities. Springer series on atomic, optical, and plasma physics 82, 1st edn. Springer International Publishing, Cham
- Eliasson B, Shukla PK (2011) Relativistic laser-plasma interactions in the quantum regime. *Phys Rev E* 83:046407. <https://doi.org/10.1103/PhysRevE.83.046407>
- Goshadze R, Berezhiani V, Osmanov Z (2019) On the filamentation instability in degenerate relativistic plasmas. *Phys Lett A* 383(10):1027–1030



- Haas F (2011) Quantum plasmas: an hydrodynamic approach. Springer series on atomic, optical, and plasma physics 65, 1st edn. Springer-Verlag, New York
- Haas F (2019) Neutrino oscillations and instabilities in degenerate relativistic astrophysical plasmas. *Phys Rev E* 99:063209. <https://doi.org/10.1103/PhysRevE.99.063209>
- Haas F, Eliasson B, Shukla PK (2012) Relativistic klein-gordon-maxwell multistream model for quantum plasmas. *Phys Rev E* 85:056411. <https://doi.org/10.1103/PhysRevE.85.056411>
- Ikramullah R, Ahmad S, Sharif FY (2017) Khattak, Nonlinear interaction of electromagnetic waves with 3-component relativistic quantum plasma. *Phys Plasmas* 24(5):052110
- Ikramullah R, Ahmad S, Sharif FY (2018) Khattak, Electron acoustic waves and parametric instabilities in a 4-component relativistic quantum plasma with thomas-fermi distributed electrons. *Phys Plasmas* 25(1):012110
- Islam S, Sultana S, Mamun AA (2017) Envelope solitons in three-component degenerate relativistic quantum plasmas. *Phys Plasmas* 24(9):092115. <https://doi.org/10.1063/1.5001834>
- Jamil M, Rasheed A, Usman M, Arshad W, Jawwad Saif M, Jung YD (2019) Karpman-washimi magnetization in relativistic quantum plasmas. *Phys Plasmas* 26(9):092110. <https://doi.org/10.1063/1.5096980>
- Marklund M, Shukla PK (2006) Nonlinear collective effects in photon-photon and photon-plasma interactions. *Rev Mod Phys* 78:591–640. <https://doi.org/10.1103/RevModPhys.78.591>
- Melrose D (2008) Quantum plasmadynamics: unmagnetized plasmas, 1st edn. Lecture notes in physics 735. Springer, Cham
- Melrose DB, Weise JI (2009) Response of a relativistic quantum magnetized electron gas. *J Phys A Math Theor* 42(34):345502
- Melrose DB, Weise JI (2012) Spin-dependent relativistic quantum magnetized electron gas. *J Phys A Math Theor* 45(39):395501
- Mendonça JT (2011) Wave kinetics of relativistic quantum plasmas. *Phys Plasmas* 18(6):062101. <https://doi.org/10.1063/1.3590865>
- Niknam A, Rastbood E, Bafandeh F, Khorashadizadeh S (2014) Modulational instability of electromagnetic waves in a collisional quantum magnetoplasma. *Phys Plasmas* 21(4):042307
- Shukla PK, Eliasson B (2011) Colloquium: nonlinear collective interactions in quantum plasmas with degenerate electron fluids. *Rev Mod Phys* 83:885–906. <https://doi.org/10.1103/RevModPhys.83.885>
- Shukla PK, Stenflo L (2006) Stimulated scattering instabilities of electromagnetic waves in an ultracold quantum plasma. *Phys Plasmas* 13(4):044505
- Singh K, Sethi P, Saini NS (2019) Nonlinear excitations in a degenerate relativistic magneto-rotating quantum plasma. *Phys Plasmas* 26(9):092104. <https://doi.org/10.1063/1.5098138>

Springer Nature or its licensor (e.g. a society or other partner) holds exclusive rights to this article under a publishing agreement with the author(s) or other rightsholder(s); author self-archiving of the accepted manuscript version of this article is solely governed by the terms of such publishing agreement and applicable law.